# Solvation of the Azide Anion ($N_3^-$) in Water Clusters and Aqueous Interfaces: A Combined Investigation by Photoelectron Spectroscopy, Density Functional Calculations, and Molecular Dynamics Simulations

**Xin Yang, Boggavarapu Kiran, Xue-Bin Wang, and Lai-Sheng Wang***

*Department of Physics, Washington State University, 2710 University Drive, Richland, WA 99352 and W. R. Wiley Environmental Molecular Sciences Laboratory, Pacific Northwest National Laboratory, MS K8-88, P.O. Box, Richland, WA 99352*

**Martin Mucha and Pavel Jungwirth**

*Institute of Organic Chemistry and Biochemistry, Academy of Sciences of the Czech Republic and Center for Complex Molecular Systems and Biomolecules, Flemingovo nam. 2, 16610 Prague 6, Czech Republic*

***To whom correspondence should be addressed. E-mail: ls.wang@pnl.gov**

## Abstract

We report a photoelectron spectroscopy and computational study of hydrated $N_3^-$ anion clusters, $N_3^-(H_2O)_n$ ($n$ = 0-16), in the gas phase. Photoelectron spectra of the solvated azide anions were observed to consist of a single peak, similar to that of the bare $N_3^-$, but the spectral width was observed to broaden as a function of cluster size due to solvent relaxation upon electron detachment. The adiabatic and vertical electron detachment energies were measured as a function of solvent number. The measured electron binding energies indicate that the first four solvent molecules have much stronger interactions with the solute anion, forming the first solvation shell. The spectral width levels off at $n$ = 7, suggesting that three waters in the second solvation shell are sufficient to capture the second shell effect in the solvent relaxation. Density functional calculations were carried out for $N_3^-$ solvated by one to five waters and showed that the first four waters interact directly with $N_3^-$ and form the first solvation shell on one side of the solute. The fifth water does not directly solvate $N_3^-$ and begins the second solvation shell, consistent with the observed photoelectron data. Molecular dynamics simulations on both solvated clusters and bulk interface revealed that the asymmetric solvation state in small clusters persist for larger systems and that $N_3^-$ prefers interfacial solvation on water clusters and at the extended vacuum/water interface.

## Introduction

As a classical example of a strong nucleophile, the azide anion is of considerable importance in organic and inorganic chemistry.[1-3] The structure and properties of $N_3^-$ have been well studied by various spectroscopic methods in the gas phase,[4-7] solution,[8-13] and crystal and solid matrices.[14-16] Theoretical calculations have also been carried out on the electronic structure of the azide anion and its behavior in solution.[17-23] Despite all the experimental and theoretical investigations in bulk solution, little information has been obtained about the microsolvation of the azide anion in water clusters, which can provide molecular level understanding about the azide-water interactions. The large values of the quadruple moment and polarizability[22] make $N_3^-$ a very special solute. One interesting issue is whether azide anion resides on the surface or in the center of a water cluster and how the solvation state evolves upon increasing the cluster size.

Gas phase photoelectron spectroscopy (PES) is an important tool for studying the energetics and dynamics of solvated anions. It has been used to study the electronic structure of hydrated electron and halide anions.[24-28] Very recently, our group has investigated the solvation of complex anions, such as $^-O_2C\text{-}(CH_2)_n\text{-}CO_2^-$ ($n$ = 2-10),[29,30] $NO_3^-$,[31] $SO_4^{2-}$,[32-34] and $C_2O_4^{2-}$,[25] using a PES apparatus coupled to an electrospray ionization (ESI) source.[36] In the current work, we report a combined study on the solvation of $N_3^-$ using PES, density functional theory (DFT) calculations, and molecular dynamics (MD) simulations. Hydrated clusters of the azide anion, $N_3^-(H_2O)_n$, were produced by an ESI source. We measured the PES spectra of the solvated species for $n$ = 0-16 at 193 nm (6.424 eV) and obtained the adiabatic and vertical electron detachment energies. The step-wise increase in the electron detachment energies revealed that the first four water molecules have strong interactions with $N_3^-$. DFT calculations were carried out, focusing on how the first few waters solvate $N_3^-$. The solvation state of $N_3^-$ in large water clusters and at the extended vacuum/water interface was investigated by MD simulations. Both

the PES data and the theoretical studies suggest an asymmetric solvation state with a surface character of the azide anion on water clusters and at extended water/vacuum interfaces.

**Experimental Method**

The experiment was carried out using an apparatus equipped with a magnetic-bottle time-of-flight (TOF) photoelectron analyzer and an ESI source. Details of the experimental method have been reported elsewhere.[36] Only a brief description is given here. A $10^{-4}$ M sodium azide solution in a water/acetonitrile (20/80 volume ratio) mixed solvent was sprayed through a 0.01 mm diameter fused quartz syringe needle biased at –2.2 kilovolts. The resulting negatively charged droplets were fed into a desolvation capillary heated to ~70 °C. Anionic species emerging from the desolvation capillary were guided by a radio-frequency quadruple system into a quadruple ion trap. The anions were accumulated in the ion trap for 0.1 second before being pushed into the extraction zone of a TOF mass spectrometer.

After mass-selection and deceleration, the $N_3^-(H_2O)_n$ anion clusters of interest were intercepted by a 193 nm (6.424 eV) laser beam from an ArF excimer laser in the detachment zone of the magnetic-bottle photoelectron analyzer. Photoelectrons were collected at nearly 100% efficiency by the magnetic bottle and analyzed in a 4-meter long TOF tube. The experiment was done at 20 Hz repetition rate with the ion beam off at alternating laser shots for background subtraction. The photoelectron TOF spectra were converted to kinetic energy spectra calibrated by the known spectra of $I^-$ and $O^-$. The electron binding energy spectra presented were obtained by subtracting the kinetic energy spectra from the detachment photon energy. The energy resolution ($\Delta E/E$) was about 2%, i.e., ~10 meV for 0.5 eV electrons, as measured from the spectrum of $I^-$ at 355 nm.

**Theoretical Methods**

We used DFT calculations to explore the structures of the small solvated clusters, $N_3^-(H_2O)_n$ ($n$ = 0–5). The final geometries were optimized using the hybrid B3LYP functional and the 6-311++G** basis set. The selection of the functional was based on a recent study, which shows that this method provides reliable data concerning the geometry and energetics of hydrated species.[37] Several initial geometries were considered. All calculations were done without any symmetry constraints using a tight geometry convergence criterion. Vertical detachment energies (VDE) were also calculated as the difference in total energy between the optimized anions and the corresponding neutral clusters at the anionic geometries. The DFT calculations were performed using the NWChem program package.[38]

Molecular dynamics simulations were performed for two systems: 1) a cluster consisting of an azide anion and sixteen water molecules and 2) an extended aqueous system in a slab geometry containing a single $N_3^-$ species in the unit cell. In the latter case, 556 water molecules and one azide anion were placed in a periodic box of dimensions 26.4 × 26.4 × 100 Å$^3$. The extension of one of the box dimensions leads to the slab arrangement of the system with two vacuum/water interfaces. For the calculations with periodic boundaries the non-bonded interactions were cut off at 12 Å and long-range electrostatic interactions were accounted for using the particle mesh Ewald procedure.[39] These simulations were performed at 300 K, while the cluster calculations were run at 250 K in order to prevent water evaporation. Both systems were first equilibrated for several hundreds of picoseconds with a subsequent 1 ns production run. The timestep was set to 1 fs and all OH bonds were constrained using the standard SHAKE procedure.[40] All MD calculations were performed using the Amber 6 program package.[41]

A polarizable force field was employed in the MD simulations. For water, we used the POL3 model.[42] For $N_3^-$ we evaluated its gas phase polarizability at the MP2/aug-cc-pvtz level. The resulting mean value of 5.85 Å$^3$ was evenly distributed on the three nitrogen atoms of the anion. For the slab calculations, the use of this value of polarizability led to the so-called

polarization catastrophe, which occurs in the case of proximal, strongly polarizable centers.[43] Therefore, we had to reduce the atomic polarizabilities on nitrogen atoms from 1.95 to 1.2 Å$^3$. At the same *ab initio* level we also evaluated the partial charges using the natural population analysis, yielding -0.62 |e| on the terminal nitrogens and +0.24 |e| on the central nitrogen atom. The van der Waals parameters of $N_3^-$ were adopted from Ref. 44.

**Results and Discussion**

**Photoelectron Spectra.** Figure 1 shows the PES spectra of $N_3^-(H_2O)_n$ ($n$ = 0-16) at 193 nm. We also took the spectrum of the bare $N_3^-$ at 355 nm with a higher energy resolution (not shown). The spectra of $N_3^-$ at both wavelengths consist of a single sharp peak,[7] indicating that there is little geometry change between the ground states of the anion and the neutral species. This result is consistent with the calculated geometries of $N_3$ and $N_3^-$.[18] The spin-orbit splitting of $N_3$ is very small (9 meV), so the width of the peak in the 193 nm spectrum (Fig. 1) is mostly due to the instrumental resolution for electrons at this kinetic energy.[7] The adiabatic electron detachment energy of $N_3^-$ measured from the 355 nm spectrum was 2.68 ± 0.03 eV, in excellent agreement with previous studies on the azide anion.[5,7] The spectra for the solvated species also consist of a single feature and shift consistently to higher binding energies with increasing solvent number. The spectra became broadened and diffuse due to solvation and the spectral width seemed to increase with increasing solvent numbers.

**Adiabatic and Vertical Detachment Energies and Evidence of the First Solvation Shell.** The adiabatic (ADE) and vertical (VDE) electron detachment energies for $N_3^-(H_2O)_n$ ($n$ = 0-16) are listed in Table I. For $N_3^-$, the ADE and VDE are identical because the geometry change between the anion and neutral is negligibly small. For the solvated clusters, the spectra became broader due to solvent relaxation upon electron detachment. Since no vibrational features were resolved, the ADE was estimated by first drawing a straight line at the leading edge of the photodetachment feature. Then a constant was added to the intersection with the

binding energy axis in order to take into account the instrumental resolution. The VDE was obtained from the peak maximum in each spectrum.

The ADE and VDE as a function of solvent number are plotted in Fig. 2a. Both curves show a monotonic increase with a clear change of slope at $n$ = 5. This turning point can be observed more clearly in the incremental increase in binding energies, as shown in Fig. 2b. The quantity, ΔADE [ADE($n$) – ADE($n$-1)], represents the electron stabilization energy with the addition of one extra solvent molecule. The first four waters clearly have the strongest stabilizing effect with ΔADE ≥ 0.34 eV (Table 1). The ΔADE suddenly drops to 0.16 eV for $n$ = 5 and steadily decreases for larger solvent numbers. The observation suggests that the first four water molecules interact strongly with $N_3^-$, evident of the first solvation shell, whereas the solute-solvent interactions become much weaker starting from the fifth water molecule, evident of the onset for the second solvation shell.

**Spectral Width and Solvent Relaxation.** The spectral width in the PES spectra represents the Franck-Condon envelope of the electronic transition between the anion and the relevant neutral state, i.e., the geometry changes between the anion ground state and the final state of the neutral species. As shown in Figure 1 and in previous studies,[7] the PES spectrum of $N_3^-$ gave a single sharp peak, indicating that there is very little geometry change upon electron detachment. However, the spectra of the solvated species became broadened and the spectral width seemed to increase with the solvent number. A good measure of the spectral width can be obtained from the difference between the ADE and VDE. These are listed in Table 1 as λ. This value increases steadily from $n$ = 0-7 and then levels off for $n$>7, reaching a value of ~0.45 eV. Since there is little geometry change upon electron detachment for $N_3^-$ itself, the spectral width of the solvated clusters should be mainly due to the solvent relaxation around the solute upon electron detachment. It is interesting to note that the solvent relaxation levels off at seven water molecules, which is beyond the first solvation shell. This observation suggests that the second solvation shell is very important for the solvent relaxation. That the additional solvent beyond $n$

= 7 does not significantly increase the relaxation energies indicates that three solvent molecules in the second solvation shell are sufficient to reproduce the effect of solvent reorganization. In other word, the $N_3^-(H_2O)_7$ cluster can be viewed as the minimal cluster size that may be used as a model for the bulk solvation.

**DFT Calculations for Small Solvated Clusters, $N_3^-(H_2O)_n$ ($n$ = 0-5).** The calculated geometries of $N_3^-(H_2O)_n$ ($n$ = 0-5) are presented in Fig. 3 along with the solute charge distributions and key bond lengths. The calculated VDE for each structure is given in Table 2. The azide anion is linear with centrosymmetric charge distribution (Fig. 3, **a**). Note that the terminal nitrogen atoms carry more than half of an electron charge. The first water forms a strong hydrogen bond with one terminal nitrogen and breaks the symmetry of the solute anion. The N…H H-bond length is extremely short (Fig. 3, **b**) and the nitrogen atom that forms the H-bond carries more charge than the nitrogen at the free end. This polarization is accompanied by a small change in the N-N bond lengths (Fig. 3, **b**). For $n$ = 2, there are two energetically degenerate solvation structures: 1) with the two water molecules solvating the two terminal N symmetrically (Fig. 3, **c1**) and 2) with both water molecules solvating only one terminal nitrogen (Fig. 3, **c2**). In the latter case, the azide anion is further polarized. In both structures, the water-N H-bonds are strong with rather short N…H bond lengths. Interestingly, for $N_3^-(H_2O)_3$ the one-end solvation structure (Fig. 3, **d1**) is slightly preferred because of the favorable water-water H-bonding.

For $N_3^-(H_2O)_4$, four low energy structures (Fig. 3, **e1**-**e4**) were obtained. The lowest energy one (**e1**) is similar to **d1** of $N_3^-(H_2O)_3$ with the fourth water forming only water-water hydrogen bonds. Thus, the maximum coordination number for one terminal nitrogen with water seems to be three, which is consistent with a previous MD simulation.[23] The second lowest energy solvation structure (**e2**) is very interesting. The four solvent molecules form a water chain along one side of the azide anion with three of them coordinating to one terminal nitrogen and the fourth water coordinating to the other terminal nitrogen. The other two structures for $N_3^-$

$(H_2O)_4$ (**e3**, **e4**) both involve solvating the two terminal N separately and are energetically unfavorable, again showing the importance of the solvent-solvent H-bonding. The "side-chain" structures turned out to be the lowest energy conformations for $N_3^-(H_2O)_5$ (Fig. 3, **f1**, **f2**), which both can be viewed as adding the fifth water to the second solvation shell of the "side-chain" structure of $N_3^-(H_2O)_4$ (**e2**). The other three conformations for $N_3^-(H_2O)_5$ (Fig. 3, **f3**, **f4** and **f5**) were all built from the low-lying isomers of $N_3^-(H_2O)_4$ and were slightly unfavored relative to **f1** and **f2**. However, as shown in Table 2 for the calculated VDEs, the lowest energy structure (**f1**) seems to be the most likely isomer responsible for the observed PES spectrum.

The calculated VDEs for all the low-lying isomers shown in Fig. 3 for $N_3^-(H_2O)_n$ ($n$ = 0-5) are given in Table 2. The calculated VDE for $N_3^-$ is in excellent agreement with the experimental measurement. However, the theoretical VDEs for the solvated species appear to be too large by between 0.17-0.26 eV for the low-lying isomers of $N_3^-(H_2O)_n$. For $n$ = 2 and 3, the two isomers are close in energy and they also have nearly identical theoretical VDEs, suggesting that they might both be populated and contribute to the PES spectra. For $N_3^-(H_2O)_4$, the two higher energy isomers (**e3**, **e4**) give VDEs that are higher than the experimental value by more than 0.3 eV and can be ruled out. It is interesting to observe that the "side-chain" structure (**e2**) gives the best VDE relative to the experimental value. For $N_3^-(H_2O)_5$, despite the near degeneracy between the two lowest-energy isomers (**f1**, **f2**), the **f1** isomer yielded the best VDE in comparison with the experimental data.

**Microsolvation of $N_3^-$ by Water**. Overall, the DFT data are in excellent agreement with the experiment. In particular, the trend of the solvation structure and the trend of the theoretical VDEs are consistent with the experimental observation. We see that, except for the **e1** structure of $N_3^-(H_2O)_4$, the first four waters interact directly with $N_3^-$ and provide the strongest stabilization, essentially forming the first solvation shell. The fifth water does not directly interact with the solute and thus exert only small stabilization to the electron binding energy of $N_3^-$. The fifth water begins to form the second solvation shell. This trend of solvation suggests

that the second solvation shell will form asymmetrically along one side of the azide anion and would lead to a surface-solvated $N_3^-$. This is consistent with our observation for the large solvated clusters and is born out from the MD simulations, as shown below.

In our previous PES studies of hydrated $SO_4^{2-}$ and $C_2O_4^{2-}$, we observed the solute photoemission features to decrease with increasing degree of solvation.[33-35] This observation was interpreted as due to the fact that the solute anion is solvated in the center of the solvated clusters. For $N_3^-(H_2O)_n$, the PES spectra contain only one solute band throughout the investigated cluster size range and it was difficult to evaluate its relative intensity change with the degree of solvation. Nevertheless, we did notice that the electron signals were quite intense for the large clusters ($n$>15) although their mass intensities decrease significantly, compared to the bare $N_3^-$ and small solvated clusters. This phenomenon was quite similar to PES spectra of hydrated $I^-$ clusters, which represent a typical system with surface solvated anions.[25,45] Therefore, our observation of strong photoemission signals for the large solvated clusters suggest that $N_3^-$ is likely to be on the surface of the large solvated clusters.

**MD Simulations of $N_3^-(H_2O)_{16}$.** Figure 4 depicts a typical snapshot from a MD simulation of a cluster consisting of 16 water molecules and a single azide anion. The snapshot clearly indicates the preferred surface solvation of $N_3^-$. This is quantified in Fig. 5, which shows the distributions of distances of water molecules and $N_3^-$ from the center of mass of the water cluster. The water signal peaks at the center with a second maximum around 3 Å, which corresponds to "outer shell" water molecules. The distribution of $N_3^-$ peaks exactly in this outer shell – a clear fingerprint of surface solvation. Results for full and reduced polarizabilities of $N_3^-$ are qualitatively similar with the anionic surface effect being slightly more pronounced for the model with full polarizability. A reduction of polarizability by 5-10% can be attributed to solvent effects.[44] However, the reduction necessary to stabilize the slab calculation is more significant (almost 40%). Nevertheless, the effect of such reduction is small and the propensity

for surface solvation is preserved. However, a non-polarizable potential model did not predict a surface solvated $N_3^-$, but rather an interior solvated structure (results not shown here).

Figure 6 shows the distribution of angles between the molecular axis of $N_3^-$ and the line connecting the center of mass of the water cluster and that of the azide anion. The angular distribution peaks at 90°, a clear indication of a preferred orientation of $N_3^-$ parallel to the cluster surface. The results for the two values of the azide polarizability almost coincide with each other. The MD results are consistent with the trend predicted from the DFT calculations for the small solvated clusters (Fig. 3) and the observation of the strong PES signals for the large solvated species. Both pointed to a surface solvated $N_3^-$ in the hydrated clusters $N_3^-(H_2O)_n$, which is born out nicely from the MD simulations.

**MD Simulation of $N_3^-$ at Extended Water/Vacuum Interfaces.** It is interesting to address the question whether the surface propensity of the azide anion persists upon moving from the hydrated clusters to extended aqueous systems. Results of MD simulation of $N_3^-$ in/on an aqueous slab are presented in Figs. 7 and 8. Figure 7 displays a density profile of $N_3^-$, i.e., a histogramed distribution of $N_3^-$ from the center of the slab to the vacuum/water interface (the interfacial region corresponds to values of the z-coordinate between roughly 10 and 14 Å). As in the cluster system, the $N_3^-$ distribution strongly peaks at the interface and clearly indicates surface solvation. Note that this result was obtained for the azide polarizability reduced by 40%. Were we able to circumvent the polarization catastrophe problem and perform the slab calculation with the full polarizability of the anion, the surface propensity of $N_3^-$ would come out even more strongly.

Finally, Figure 8 shows the distribution of angles between the molecular axis of $N_3^-$ and the normal to the surface of the slab. Similar to the cluster system, the angular distribution peaks around 90°. A close inspection of the trajectory reveals that the orientation of $N_3^-$ is strongly correlated with the position of the anion in the slab. On one hand, when the azide anion is at the water/vacuum interface (which is most of the time) it is almost exclusively oriented parallel to

the surface. On the other hand, during the short periods when $N_3^-$ "dives" into the subsurface or aqueous bulk, its orientation tends to get randomized, which would be expected if the solvent environment is more or less symmetric.

We note that the behavior of $N_3^-$ at the bulk interface is well represented using a solvated cluster. Both the DFT and MD results confirm the experimental inference of four waters as the first solvation shell of $N_3^-$. Since the solvent relaxation levels off at seven waters as observed in the PES data, the MD results also verify the notion that a seven-water cluster can be used as the bare minimum to describe the solvation behavior of $N_3^-$ using cluster models.

**Conclusions**

Gas phase photoelectron spectroscopic and computational studies of water-solvated azide anion clusters, $N_3^-(H_2O)_n$ ($n$ = 0-16), were reported. PES spectra of bare and solvated $N_3^-$ were taken at 6.424 eV (193 nm). The spectral features of the solvated clusters are similar to that of the bare $N_3^-$, except that they become broadened and shifted to the blue due to solvation. The spectral width increases with the solvation number and levels off at $n$ = 7. The adiabatic and vertical electron binding energies were measured for each species. The step-wise electron stabilization energies indicated that the first four solvent molecules have the strongest interaction with the solute anion. DFT calculations show how the first five solvent molecules solvate $N_3^-$ one water at a time. The first four water molecules were found to directly coordinate to $N_3^-$ along one side of the linear anion forming the first solvation shell asymmetrically; the fifth water has no direct interactions with the solute and begins the second solvation shell, in agreement with the experimental observation. The leveling off of the spectral width at $n$ = 7 suggests that three waters in the second solvation shell are sufficient to capture the solvent relaxation effect upon electron detachment. The asymmetric solvation state in the small clusters was shown to persist in larger solvation systems using MD simulations. MD simulations with a polarizable force field

reveal that $N_3^-$ anion clearly prefers interfacial over bulk solvation in large clusters and at the extended vacuum/water interface.

**Acknowledgements**

This work was supported by The U.S. Department of Energy (DOE), Office of Basic Energy Sciences, Chemical Science Division, and was performed at the W. R. Wiley Environmental Molecular Sciences Laboratory, a national scientific user facility sponsored by DOE's Office of Biological and Environmental Research and located at Pacific Northwest National Laboratory, operated for DOE by Battelle. Support from the Czech Ministry of Education via a grant No. ME644 is gratefully acknowledged.

**References**


1. Patai, S. *The Chemistry of the Azido Group* (Interscience: London, **1971**).
2. Fair, H. D.; Walker, R. F. *Energ. Mater*. **1997**, *1*.
3. Ingold, C. K. *Structure and Mechanism in Organic Chemistry* (Cornell University Press: Ithaca, New York, **1969**).
4. Jackson, R. L.; Pellerite, M. J.; Brauman, J. I. *J. Am. Chem. Soc*. **1981**, *103*, 1802.
5. Polak, M.; Gruebele, M.; Saykally, R. J. *J. Am. Chem. Soc.* **1987**, *109*, 2884.
6. Owrutsky, J. C.; Rosenbaum, N.; Tack, T.; Gruebele, M.; Polak, M.; Saykally, R. J.; *Philos. Trans. R. Soc. London A* **1988**, *324*, 23.
7. Continetti, R. E.; Cyr, D. R.; Metz, R. B.; Neumark, D. M. *Chem. Phys. Lett*. **1991**, *182*, 406.
8. Dean, K. J.; Wilkinson, G. R. *J. Raman Spectrosc*. **1985**, *16*, 22.
9. Li, M.; Owrutsky, J. C.; Sarisky, M. J.; Culver, J. P.; Yodh, A.; Hochstrasser, R. M.; *J. Chem. Phys*. **1993**, *98*, 5499.
10. Hamm, P.; Lim, M.; Hochstrasser, R. M. *Phys. Rev. Lett*., **1998**, *81*, 5326.
11. Le Borgne, C.; Illien, B.; Beignon, M.; Chabane, M. *Phys. Chem. Chem. Phys*. *1999*, ***1***, 4701.
12. Waterland, M. R.; Kelley, A. M. *J. Phys. Chem. A* **2001,** *105*, 8385.
13. Zhong, Q.; Steinhurst, D. A.; Carpenter, E. E.; Owrustsky, J. C. *Langmuir* **2002***, 18*, 7401.
14. Sherman, W. F.; Wilkinson, G. R. *Vibrational Spectroscopy of Trapped Species*; Hallam, H. E. Ed. pp 245-354. (Wiley: London, **1973**)
15. Zhou, M.; Andrew, L. *J. Phys. Chem. A* **2000**, *104*, 1648.
16. Andrew, L.; Zhou, M.; Chertihin, G. V.; Bare, W. D.; Hannachi, Y. *J. Phys. Chem. A* **2000,** *104*, 1656.
17. Peyerimhoff, S. D.; Buencker, R. J. *J. Chem. Phys.* **1967,** *47*, 1953.
18. Archibald, T. W.; Sabin, J. R. *J. Chem. Phys*. **1971**, *55*, 1821.

19. Gora, T.; Kemmey, P. J. *J. Chem. Phys*. **1972**, *57*, 3579.

20. Rossi, A. R.; Bartram, R. H. *J. Chem. Phys*. **1979**, *70*, 532.

21. Botschwina, P. *J. Chem. Phys*. **1986**, *85*, 4591.

22. Morita, A.; Kato, S. *J. Chem. Phys*. **1998**, *109*, 5511.

23. Yarne, D. A.; Tuckerman, M. E.; Klein, M. L. *Chem. Phys*. **2000**, *258*, 163.

24. Coe, J. V.; Lee, G. H.; Eaton, J. G.; Arnold, S. T.; Sarkas, H. W.; Bowen, K. H. *J. Chem. Phys*. **1990,** *92*, 3980.

25. Markovich, G.; Pollack, S.; Giniger, R.; Cheshnovsky, O. *J. Chem. Phys*. **1994**, *101*, 9344 .

26. Kim, J.; Becker, I.; Cheshnovsky, O.; Johnson, M. A. *Chem. Phys. Lett*. **1998**, *297*, 90.

27. Lehr, L.; Zanni, M. T.; Frischkorn, C.; Weinkauf, R.; Neumark, D. M. *Science* **1999**, *284*, 635.

28. Yang, X; Wang, X. B.; Wang, L. S. *J. Chem. Phys*. **2001**, *115*, 2889.

29. Ding, C. F.; Wang, X. B.; Wang, L. S. *J. Phys. Chem. A* **1998,** *102*, 8633.

30. Yang, X.; Fu, Y. J.; Wang, X. B.; Slavicek, P.; Muncha, M.; Jungwirth, P.; Wang, L. S. *J. Am. Chem. Soc*. **2004**, *126*, 876.

31. Wang, X. B.; Yang, X.; Wang, L. S.; Nicholas, J. B. *J. Chem. Phys.* **2002,** *116*, 561.

32. Wang, X. B.; Nicholas, J. B.; Wang, L. S. *J. Chem. Phys*. **2000**, *113*, 10837.

33. Wang, X. B.; Yang, X.; Nicholas, J. B.; Wang, L. S. *Science* **2001**, *294*, 1322.

34. Yang, X.; Wang, X. B.; Wang, L. S. *J. Phys. Chem. A* **2002,** *106*, 7607.

35. X. B. Wang, X. Yang, J. B. Nicholas, L. S. Wang, J. Chem. Phys. **119**, 3631 (2003).

36. Wang, L. S., Ding, C. F.; Wang, X. B.; Barlow, S. E. *Rev. Sci. Instrum*. **1999**, *70*, 1957.

37. Tuma, C.; Boese, A. D.; Handy, N. C. *Phys. Chem. Chem. Phys.* **1999**, *1***,** 3939.

38. High Performance Computational Chemistry Group, *NWChem, A Computational Chemistry Package for Parallel Computers, Version 4.5*; Pacific Northwest National Laboratory, Richland, Washington 99352, USA. **2003**.

39. Essmann, U.; Perera, L.; Berkowitz, M. L.; Darden, T.; Pedersen, L. G. *J. Chem. Phys*. **1995**, *103*, 8577.

40. Ryckaert, J. P.; Ciccotti, G.; Berendsen, H. J. C.; Comput. J. *Phys*. **1997**, *23*, 327.

41. Case, D. A.; Pearlman, D. A.; Caldwell, J. W.; Cheatham III, T. E.; Ross, W. S.; Simmerling, C. L.; Darden, T. A.; Merz, K. M.; Stanton, R. V.; Cheng, A. L.; Vincent, J. J.; Crowley, M.; Tsui, V.; Radmer, R. J.; Duan, Y.; Pitera, J.; Massova, I.; Seibel, G. L.; Singh, U. C., AMBER6, University of California, San Francisco, **1999**.

42. Caldwell, J. W.; Kollman, P. A. *J. Phys. Chem*. **1995**, *99,* 6208.

43. Thole, B. T. *Chem. Phys*. **1981**, *59*, 341.

44. Morita, A.; Kato, S. *J. Chem. Phys*. **1998**, *109*, 5511.

45. Coe, J. V. *J. Phys. Chem. A* **1997,** *101*, 2055.

**TABLE 1**: Adiabatic (ADE) and Vertical (VDE) Electron Detachment Energies for $N_3^-(H_2O)_n$ ($n$ = 0-16) in eV.[a]

| $n$ | ADE | ΔADE[b] | VDE | ΔVDE[c] | λ[e] |
|---|---|---|---|---|---|
| 0 | 2.68 (3)[d] | | 2.68 (3)[d] | | 0 |
| 1 | 3.14 (6) | 0.46 (6) | 3.25 (6) | 0.57 (6) | 0.11 |
| 2 | 3.58 (6) | 0.44 (6) | 3.78 (6) | 0.53 (6) | 0.20 |
| 3 | 4.04 (6) | 0.46 (6) | 4.25 (6) | 0.47 (6) | 0.21 |
| 4 | 4.38 (6) | 0.34 (6) | 4.63 (6) | 0.38 (6) | 0.25 |
| 5 | 4.54 (6) | 0.16 (6) | 4.85 (6) | 0.22 (6) | 0.31 |
| 6 | 4.70 (8) | 0.16 (8) | 5.03 (8) | 0.18 (8) | 0.33 |
| 7 | 4.84 (8) | 0.14 (8) | 5.25 (8) | 0.22 (8) | 0.41 |
| 8 | 4.98 (8) | 0.14 (8) | 5.42 (8) | 0.17 (8) | 0.44 |
| 9 | 5.12 (8) | 0.14 (8) | 5.55 (8) | 0.13 (8) | 0.43 |
| 10 | 5.25 (8) | 0.13 (8) | 5.65 (8) | 0.10 (8) | 0.40 |
| 11 | 5.34 (8) | 0.09 (8) | 5.70 (8) | 0.05 (8) | 0.36 |
| 12 | 5.37 (8) | 0.03 (8) | 5.79 (8) | 0.09 (8) | 0.42 |
| 13 | 5.45 (8) | 0.08 (8) | 5.89 (8) | 0.10 (8) | 0.44 |
| 14 | 5.49 (8) | 0.04 (8) | 5.95 (8) | 0.06 (8) | 0.46 |
| 15 | 5.58 (8) | 0.09 (8) | 6.02 (8) | 0.07 (8) | 0.44 |
| 16 | 5.62 (8) | 0.04 (8) | 6.07 (8) | 0.05 (8) | 0.45 |

[a] The numbers in the parentheses represent the uncertainties in the last digit.
[b] ADE($n$) – ADE($n$-1).
[c] VDE($n$) – VDE($n$-1).
[d] The EA of $N_3$ measured from the 355 nm spectrum. This value was measured to be 62.1 ± 2.8 kcal/mol (2.69 ± 0.12 eV) from Ref. 4 and 2.68 ± 0.01 eV from Ref. 7.
[e] (VDE – ADE).

**TABLE 2**: The Calculated Vertical Detachment Energies (VDE) for $N_3^-(H_2O)_n$ ($n$ = 0-5) in eV Compared with the Experimental Value from Table 1. See Figure 3 for the Labels of the Isomers.

| *n* | isomers | VDE (theo.) | VDE (exp.)[a] |
|---|---|---|---|
| 0 | **a** | 2.72 | 2.68 (3) |
| 1 | **b** | 3.42 | 3.25 (3) |
| 2 | **c1** | 4.04 | 3.78 (6) |
| | **c2** | 4.05 | |
| 3 | **d1** | 4.49 | 4.25 (6) |
| | **d2** | 4.52 | |
| 4 | **e1** | 4.87 | 4.63 (6) |
| | **e2** | 4.82 | |
| | **e3** | 4.97 | |
| | **e4** | 4.96 | |
| 5 | **f1** | 4.96 | 4.85 (6) |
| | **f2** | 5.17 | |
| | **f3** | 5.24 | |
| | **f4** | 5.36 | |
| | **f5** | 5.31 | |

a. Reproduced from Table 1.

**Figure Captions**

**Fig. 1** Photoelectron spectra of $N_3^-(H_2O)_n$ ($n$ = 0-16) at 193 nm (6.424 eV).

**Fig. 2** **(a)** Adiabatic (ADE) and vertical (VDE) detachment energies of $N_3^-(H_2O)_n$ ($n$ = 0-16) as a function of solvent number ($n$). **(b)** The incremental increase of electron detachment energies, ΔADE = ADE($n$) - ADE($n$-1) and ΔVDE, as a function of solvent number ($n$).

**Fig. 3** Optimized structures for the lowest energy isomers of $N_3^-(H_2O)_n$ ($n$ = 0-5 ) at B3LYP/6-311++G**. Relative energies are given in eV. Mulliken charges on the nitrogen atoms are also given, along with key bond lengths in angstrom.

**Fig. 4** A typical snapshot from a MD simulation of a cluster consisting of 16 water molecules and a single azide anion. Color coding: nitrogen – blue, oxygen – red, and hydrogen – white.

**Fig. 5** Distributions of distances of water molecules and $N_3^-$ from the center of mass of the water clusters in $N_3^-(H_2O)_{16}$. Model 1: full polarizability of 1.95 $Å^3$ on nitrogen atoms. Model 2: polarizability on nitrogen atoms reduced to 1.2 $Å^3$.

**Fig. 6** Distribution of angles between the molecular axis of $N_3^-$ and the line connecting the center of mass of the water cluster and that of the azide anion in $N_3^-(H_2O)_{16}$. Model 1: full polarizability of 1.95 $Å^3$ on nitrogen atoms. Model 2: polarizability on nitrogen atoms reduced to 1.2 $Å^3$.

**Fig. 7** The density profile of the azide anion from the center of an aqueous slab to the vacuum/water interface. The interfacial region lies between 10 and 14 Å.

**Fig. 8** Distribution of angles between the molecular axis of the $N_3^-$ and the normal to the surface of the slab.

**Figure 1**

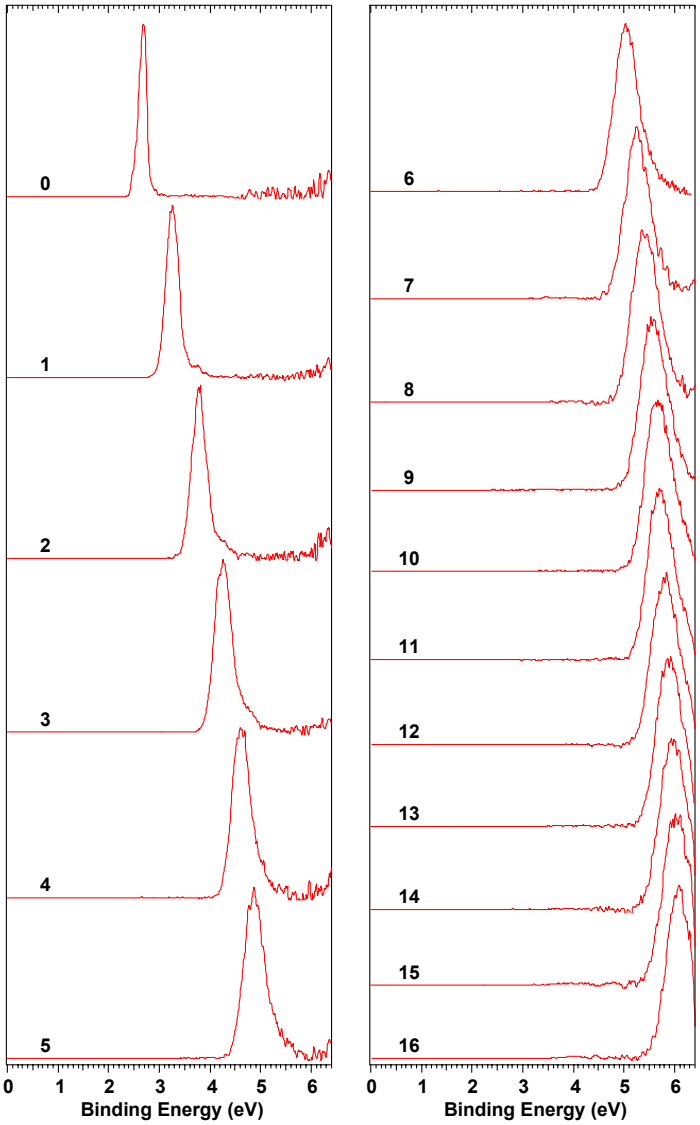
0
1
2
3
4
5
6
7
8
9
10
11
12
13
14
15
16
0 1 2 3 4 5 6
Binding Energy (eV)
0 1 2 3 4 5 6
Binding Energy (eV)

**Figure 2**

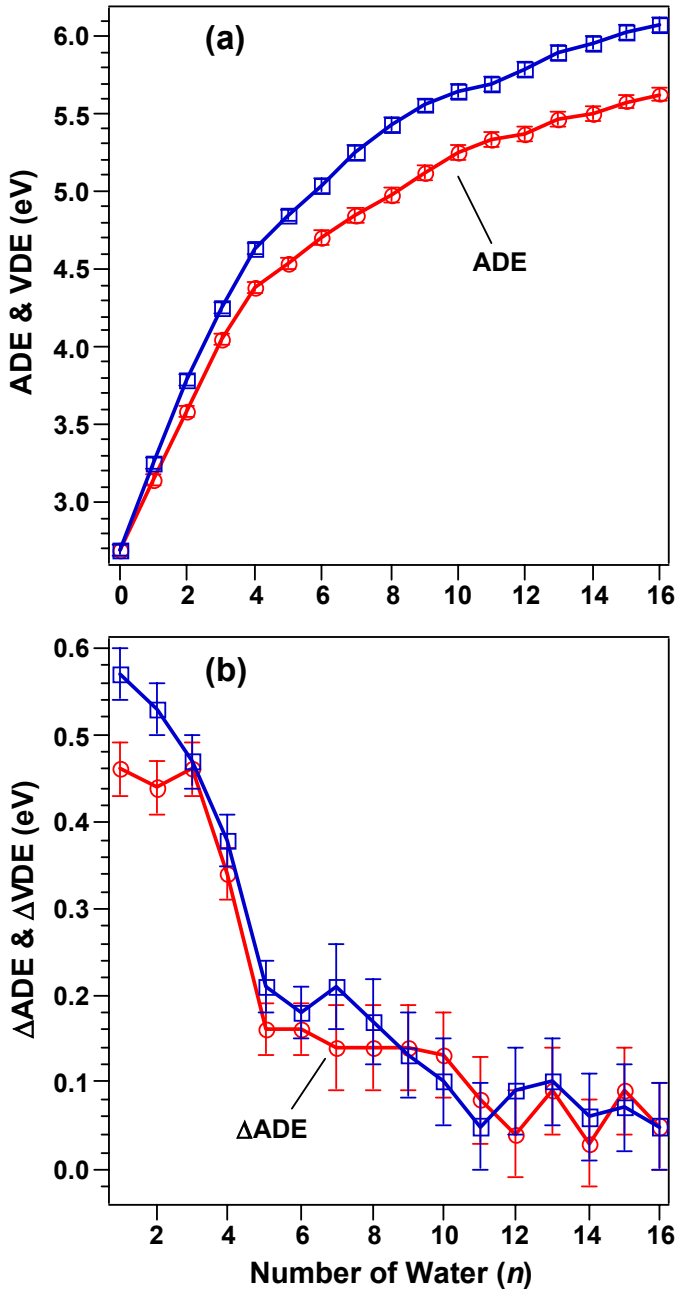
(a)
ADE & VDE (eV)
6.0
5.5
5.0
4.5
4.0
3.5
3.0
ADE
0
2
4
6
8
10
12
14
16
(b)
ΔADE & ΔVDE (eV)
0.6
0.5
0.4
0.3
0.2
0.1
0.0
ΔADE
2
4
6
8
10
12
14
16
Number of Water (n)

**Figure 3**

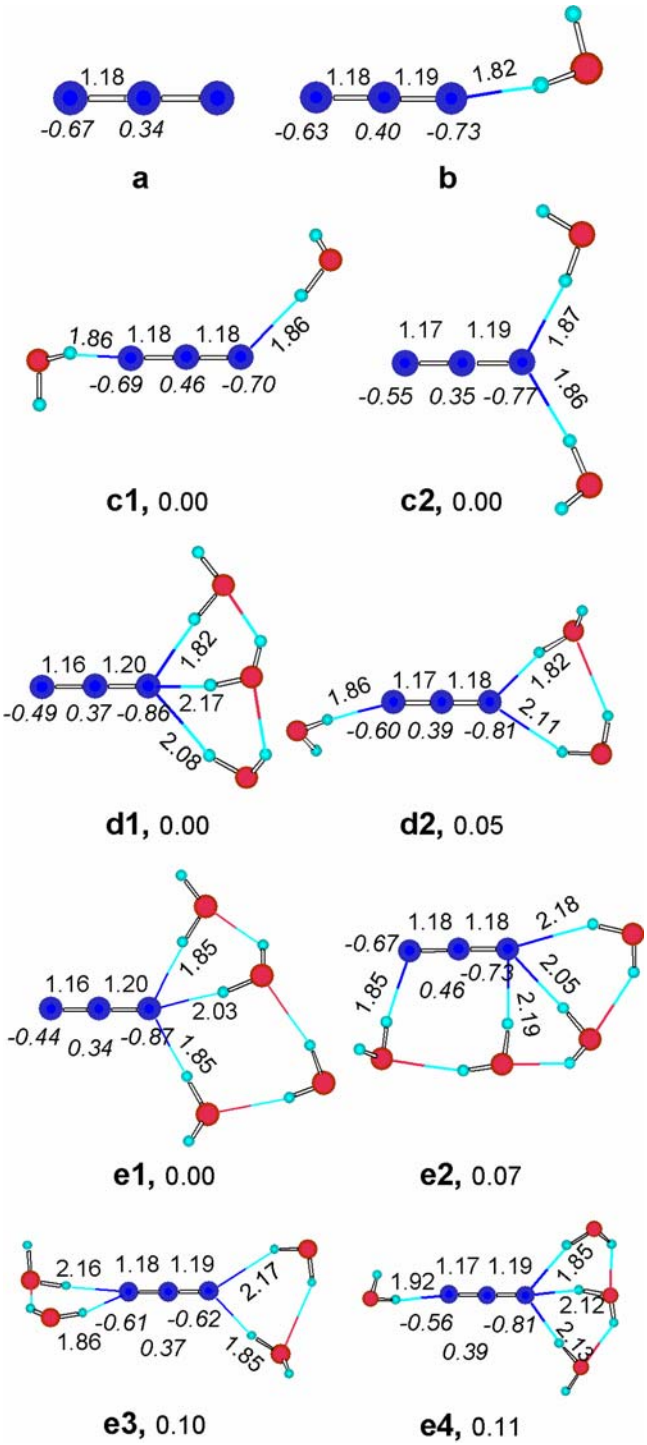
1.18
-0.67 0.34
a
1.18 1.19 1.82
-0.63 0.40 -0.73
b
1.86 1.18 1.18 1.86
-0.69 0.46 -0.70
c1, 0.00
1.17 1.19 1.87
-0.55 0.35 -0.77 1.86
c2, 0.00
1.16 1.20 1.82
-0.49 0.37 -0.86 2.17
2.08
d1, 0.00
1.86 1.17 1.18 1.82
-0.60 0.39 -0.81 2.11
d2, 0.05
1.16 1.20 1.85
2.03
-0.44 0.34 -0.87 1.85
e1, 0.00
1.18 1.18 2.18
-0.67 -0.73 2.05
1.85 0.46 2.19
e2, 0.07
2.16 1.18 1.19 2.17
-0.61 -0.62
1.86 0.37 1.85
e3, 0.10
1.92 1.17 1.19 1.85
2.12
-0.56 -0.81
0.39
e4, 0.11

**Figure 3 (continued)**

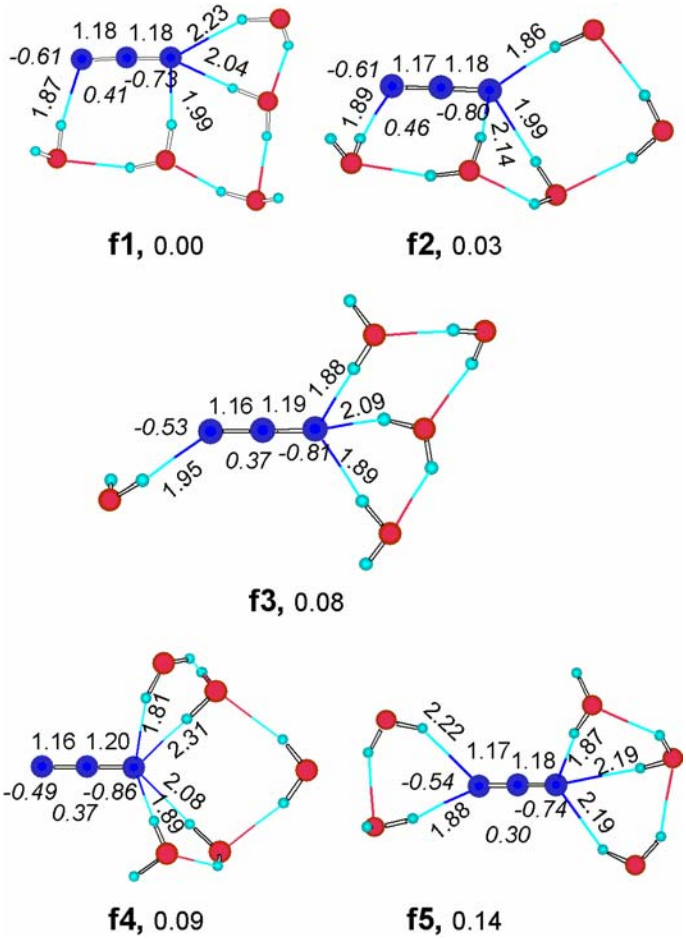

**Figure 4**

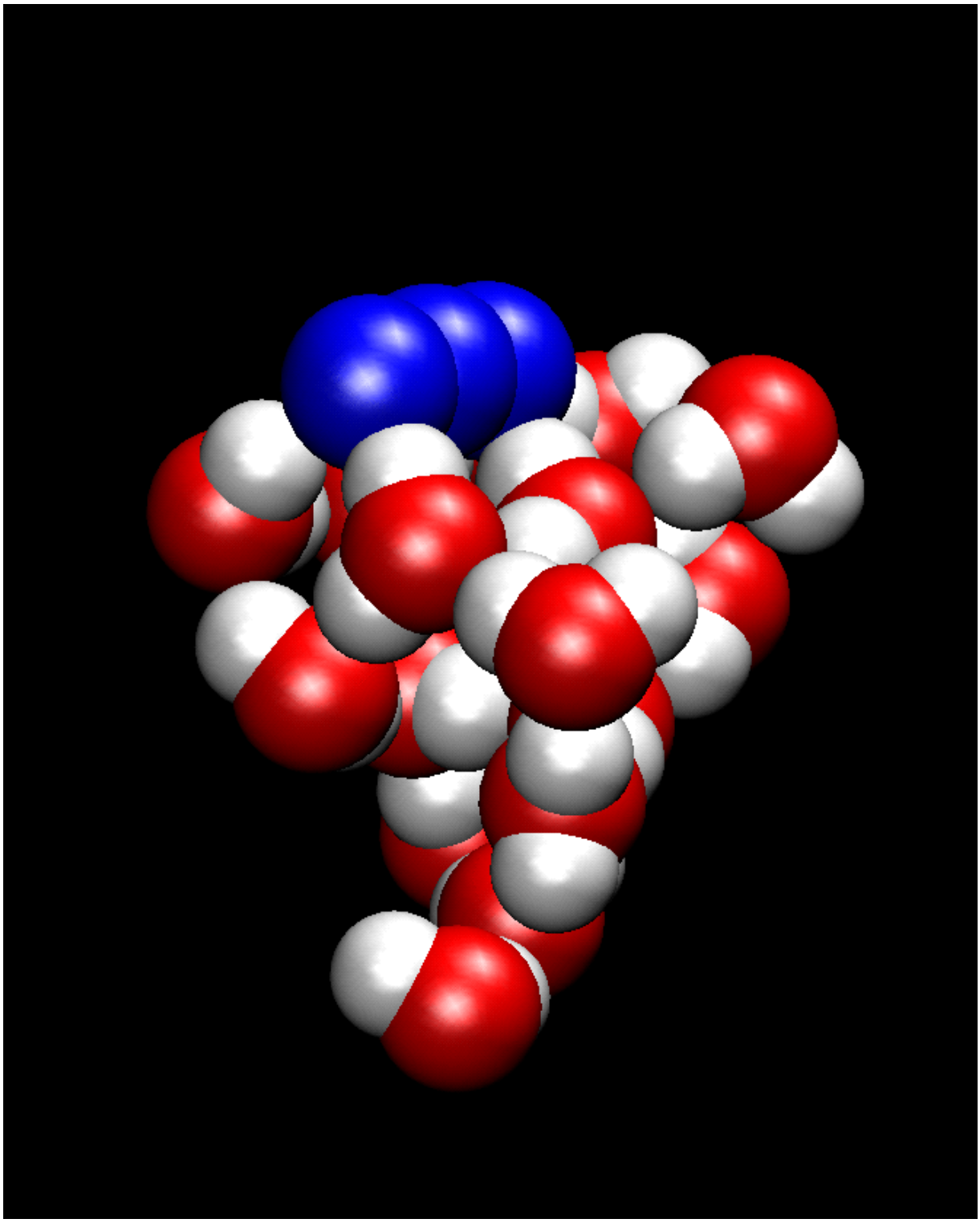

**Figure 5**

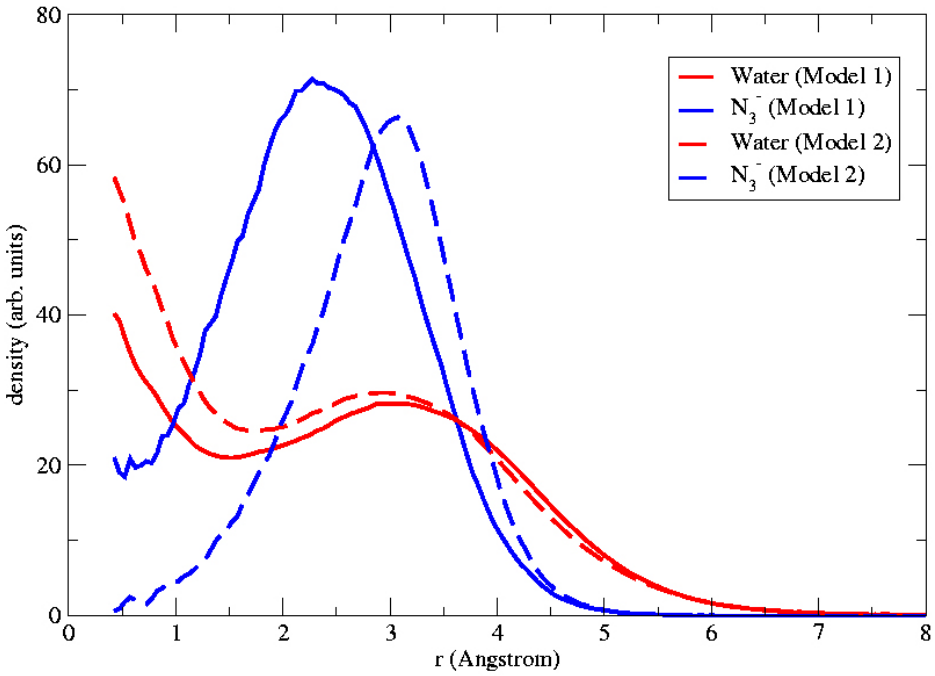
Water (Model 1)
N3- (Model 1)
Water (Model 2)
N3- (Model 2)
density (arb. units)
r (Angstrom)
0
20
40
60
80
0
1
2
3
4
5
6
7
8

**Figure 6**

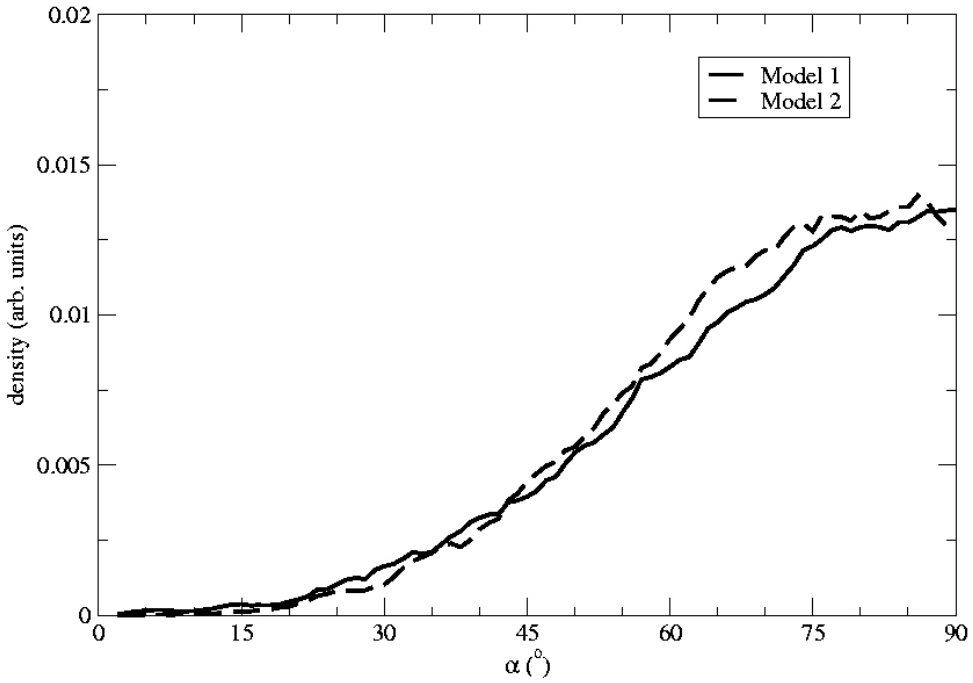
0.02
0.015
0.01
0.005
0
density (arb. units)
0
15
30
45
60
75
90
α (°)
Model 1
Model 2

**Figure 7**

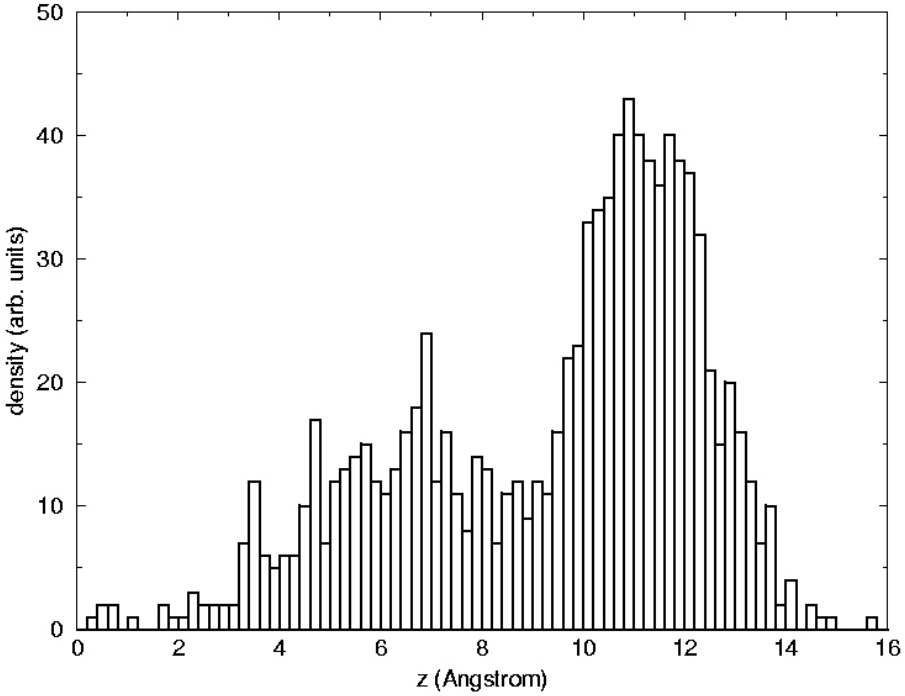

**Figure 8**